Annular Plate under a Transverse Line Impulse

ALEXANDER L. FLORENCE*
Stanford Research Institute, Menlo Park, Calif.

This paper contains three approximate solutions for finding the permanent edge deflection of an annular plate. The plate, clamped at the inner boundary, free at the outer, is subjected to a uniform transverse impulse on a narrow annular area at the outer edge. The material is assumed to have a rigid-plastic behavior and to deform according to the Tresca yield condition and associated flow rule. Since the problem is complicated when bending and membrane actions are included, it is represented as one of three less complicated subproblems, each of which is then made tractable by means of approximations. In the first of these, the usual procedure of considering bending alone is adopted. In the second, yielding is assumed to occur in the form of a limited interaction, that between the circumferential components of bending moment and membrane force. In the third, membrane forces alone are considered. Finally, experiments are described, and the results in the form of plate edge deflections are compared with the three different theoretical predictions. For large deflections, results indicate a great improvement over the bending theory when membrane action is included.

Introduction

THE problem treated here is the determination of the permanent deformation of an annular plate that is clamped at its inner boundary of radius a and free at its outer boundary of radius R, where a uniform transverse impulse is applied on a narrow annular area of width $R - R_0$ (Fig. 1). The material is assumed to have a rigid-plastic behavior and to deform according to the Tresca yield condition and associated flow rule. In view of the complications that arise when both bending and membrane actions occur as the plate deforms, the problem is represented in turn as one of three less complicated subproblems. In the first of these it is assumed that the bending action predominates so that the membrane forces are neglected. This is called the bending solution. In the second, some account is taken of the membrane action of the plate by assuming that the yield condition involves an interaction between the circumferential components of the bending moment and membrane force. This is called the limited interaction solution. Finally, the third problem assumes predominance of membrane forces so that the bending moments are neglected. This is called the membrane solution.

In each case the same mechanism of deformation is used, consisting of a traveling plastic hinge circle originating at the edge of the loading at radius $r = R_0$ and ending at the clamped support at $r = a$. After this first phase of motion the hinge circle is assumed to remain at the support until the plate motion ceases. A further simplification is achieved in the second and third problems, in which membrane forces are acting, if, for the purposes of deriving the momentum equations, the annular part of the plate outside of the hinge circle is approximated by a shallow cone. This assumption was suggested by the final deformed shapes obtained in experiments that will be described later.

An approximation common to all of the solutions is that the initial velocity distribution plotted along a radius is zero for $a \leq r \leq R_0$ and triangular for $R_0 \leq r \leq R$, going from zero at $r = R_0$ to a maximum at $r = R_s$, such that the momentum equals applied impulse. During motion the velocity distribution remains triangular, since elemental sectors of plate are assumed to rotate as rigid bodies about their intersection with the hinge circle.

All of the preceding assumptions are made to simplify the analysis and to allow the derivation of formulas for the permanent deflection that may be useful for engineering applications. The predicted deflections are compared with those from experiments in which aluminum plates are subjected around their rims to impulses generated by explosive.

Bending Solution

Hopkins and Prager[1] and Wang and Hopkins[2] have thoroughly examined the subject of dynamic plastic deformation of circular plates of rigid-plastic material, obeying the Tresca yield condition and the associated flow rule. In these references, the bending action was assumed to predominate over the membrane action, and so the latter was neglected. Consequently, many of the established results, such as continuity conditions at traveling hinge circles, can be taken over. Shapiro[3] has treated an annular plate problem similar to that given here but with the rim given a constant velocity for a short time.

The mechanism of plate deformation assumes that at time $t = 0$, the time of application of the impulse, a plastic hinge circle forms at radius $r = R_0$, whereupon it travels inward to arrive at the support at time $t = t_s$, and occupies position $r = \rho(t)$ for $0 < t < t_s$ (Fig. 2). During this first phase the hinge circle H divides the plate into two annular regions. In the inner region $a \leq r \leq \rho(t)$ the material is assumed to be undeformed with the governing plastic regime given by A in Fig. 3 that expresses the Tresca yield condition in terms of the radial and circumferential components of bending moment M_r and M_θ. (Positive when tendency is to cause tension in the upper layer of the plate.)

Consequently, in the region

$$a \leq r \leq \rho(t) \qquad M_r = M_\theta = M_0 \qquad \dot{\varkappa}_r = \varkappa_\theta = 0 \quad (1)$$

where $M_0 = \sigma_0 d^2/4$ is the fully plastic moment, σ_0 being the static yield stress, d the thickness of the plate, and $\dot{\varkappa}_r$ and $\dot{\varkappa}_\theta$, the radial and circumferential rates of curvature change. In the outer region, $\rho(t) \leq r \leq R$, elemental sectors rotate as rigid bodies about their line of intersection with the hinge circle. From this assumed mechanism, the yield condition and the associated flow rule are

$$0 \leq M_r \leq M_0 \qquad M_\theta = M_0 \qquad \dot{\varkappa}_r = 0 \qquad \dot{\varkappa}^\theta \neq 0 \quad (2)$$

The expressions (2) correspond to the plastic regime AB in Fig. 3, with A at $r = \rho$ where $M_r = M_0$ and B at $r = R$ where

Received November 19, 1964; revision received April 2, 1965. This research was sponsored by the U. S. Air Force through the Air Force Weapons Laboratory under Contract No. AF 29(601)-4329. The author is indebted to R. Firth, B. Reese, and M. Lynch who carried out the experiments, to B. Bain for the numerical work, to G. R. Abrahamson and H. E. Lindberg for helpful advice and criticism, and to M. Stallybrass for his contribution to the bending solution.

* Research Engineer, Poulter Research Laboratories.

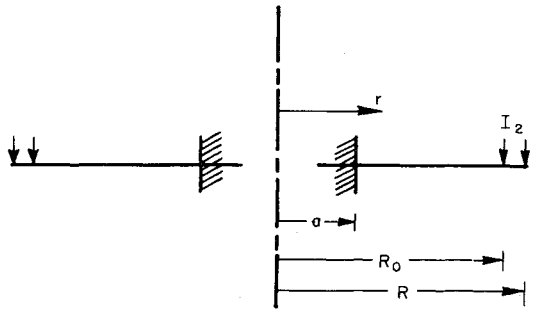

Fig. 1 Annular plate problem.

$M_r = 0$. Letting the angular velocity about H of each elemental sector be ω, the velocity distribution during phase 1 is

$$\dot{w}(r, t) = \begin{cases} \omega(r - \rho) & \rho \leq r \leq R \\ 0 & a \leq r \leq \rho \end{cases} \tag{3}$$

where $w(r, t)$ is the displacement, and the dot denotes time differentiation.

The second phase starts at time $t = t_s$ when $\rho(t_s) = a$, and the insuing mechanism of deformation assumes a stationary plastic hinge circle at the support with the deformed elemental sectors rotating about it as rigid bodies. Hence, the velocity distribution is

$$\dot{w}(r_a, t) = \omega(r - a) \qquad a \leq r \leq R \tag{4}$$

and, from the Tresca yield condition and flow rule,

$$0 \leq M_r \leq M_0 \qquad M_\theta = M_0 \qquad \dot{\varkappa}_r = 0 \qquad \dot{\varkappa}_\theta \neq 0 \tag{5}$$

In this phase the whole plate is in the plastic regime AB.

The initial conditions for the first phase are

$$w(r, o) = 0 \qquad a \leq r \leq R$$
$$\dot{w}(r, o) = \begin{cases} 0 & a \leq r \leq R_0 \\ V(r - R_0)/(R - R_0) & R_0 \leq r \leq R \end{cases} \tag{6}$$

in which V, the initial velocity of the edge of the plate, is determined as follows. Let I_2 be the impulse applied per unit area in the annular region $R_0 \leq r \leq R$. Then, equating the initial momentum per unit sector of plate given by (6) to the impulse from I_2 on the sector leads to $V = 3I_2(R + R_0)/m(2R + R_0)$, where m is the mass per unit area of plate.

With the aid of relations (1–6), equations can be written for conservation of linear momentum and of angular momentum about $r = a$ of a unit sector of the plate. In a convenient form these are, during phase 1,

$$\omega = 3I_2(R^2 - R_0^2)/m(R - \rho)^2(2R + \rho) \tag{7}$$

$$M_0R = m[\omega\rho F(\rho) - \dot{\omega}G(\rho)] \tag{8}$$

where

$$F(\rho) = (R - \rho)[2(R - \rho)^2 - 3(R - \rho)(2R - a) + 6R(R - a)]/6 \tag{9}$$

$$G(\rho) = (R - \rho)^2[(R - \rho)^2 - 2(R - \rho)(2R - a) + 6R(R - a)]/12 \tag{10}$$

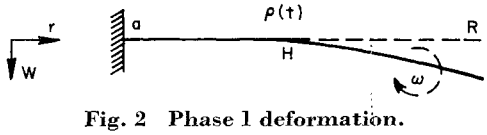

Fig. 2 Phase 1 deformation.

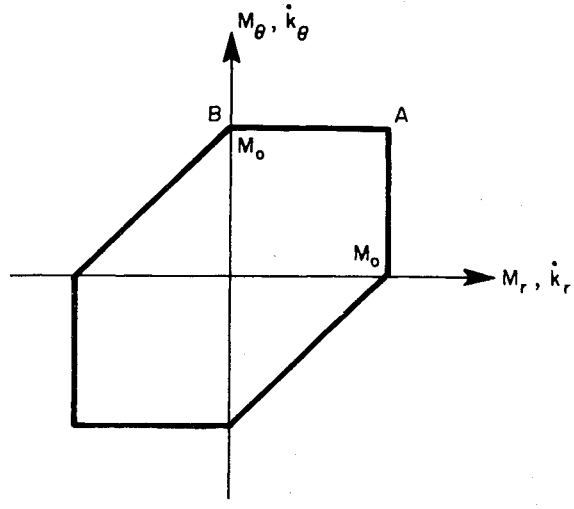

Fig. 3 Tresca yield hexagon.

Differentiating (7) with respect to time and substituting the resulting expression for the angular acceleration $\dot{\omega}$, along with that for ω from (7), in (8) gives the velocity $\dot{\rho}$ of the hinge circle as a function of ρ. This relationship is

$$M_0R = -I_2^2(R^2 - R_0^2)\dot{\rho}H/4(2R + \rho)^2 \tag{11}$$

in which

$$H = (R - \rho)^2 - 6R(R - \rho) + 6R^2$$

At time $t = t_s$, when the hinge circle reaches the support, the rotation of the elements of an elemental sector of the plate is

$$\theta(r, t_s) = \int_\tau^{t_s} \omega(t)\cdot dt = \int_r^a \frac{\omega(\rho)d\rho}{\dot{\rho}} =$$
$$\frac{3I_2^2(R^2 - R_0^2)^2\,[(3R + r)/(R - r)(2R + r)^2 - (3R + a)/(R - a)(2R + a)^2]}{8mM_0R} a \leq r \leq R_0 \tag{12}$$

In (12), τ is the time when the hinge circle reaches the element at radius r. To evaluate the integral in (12), formulas (7) and (11) were used to give ω and $\dot{\rho}$ as functions of ρ. Assuming $\theta(r, t_s)$ small enough to allow the approximation $\theta(r, t_s) = \partial w/\partial r$, the integration of (12) with respect to r yields the following deflection curve for $a \leq r \leq R_0$:

$$w(r, t_s) = I_2^2(R^2 - R_0^2)^2\{\log[(2R + r)(R - a)/(2R + a)(R - r)] + 3R(r - a)/4(2R + r)(2R + a) - 9R(3R + a)(r - a)/4(2R + a)^2(R - a)\}/6mM_0R^2 \tag{13}$$

During the second phase, the conservation of angular momentum equation is

$$M_0R = -m\dot{w}G(a) \tag{14}$$

where, according to (10), $G(a) = (R - a)^3(3R + a)/12$. In this phase, every element is rotating with the same angular velocity ω. Integrating (14) with respect to time gives $\omega = \omega(t_s) - M_0R(t - t_s)/mG$, where $\omega(t_s)$ is obtained by substituting $\rho = a$ in (7). Letting $t = t_f$ be the time when motion ceases so that $\omega(t_f) = 0$ gives $t_f - t_s = \omega(t_s)mG/M_0R$. Hence, one further integration yields the rotation of the elements in phase 2, that is,

$$\theta(r, t_f) - \theta(r, t_s) = \frac{3I_2^2(R^2 - R_0^2)^2(3R + a)}{8mM_0R(R - a)(2R + a)^2} \tag{15}$$

The deflection during phase 2 is approximately $[\theta(r, t_f) - \theta(r, t_s)](r - a)$. Adding this value to (13) gives the final

displacement as

$$w(r, t_f) = I_2^2(R^2 - R_0^2)^2\{\log[(2R + r)(R - a)/(2R + a)(R - r)] + 3R(r - a)/4(2R + a)(2R + r)\}/6mM_0R^2 \qquad a \leq r \leq R_0 \quad (16)$$

Let δ be the final edge deflection. Then

$$\delta = w(R_0, t_f) + (R - R_0)\theta(R_0, t_f) \quad (17)$$

By substituting $w(R_0, t_f)$ from (16) and $\theta(R_0, t_f)$ from (15) and (12) in Eq. (17), the expression for the edge deflection becomes

$$\delta = I_2^2(R^2 - R_0^2)^2\{(1/3R)\log[(2R + R_0)(R - a)/(2R + a)(R - R_0)] + (R_0 - a)/4(2R + a)(2R + R_0) + 3(3R + R_0)/4(2R + R_0)^2\}/2mM_0R \quad (18)$$

Limited Interaction Solution

This is the case in which membrane and bending effects are comparable. Each elemental sector of plate is assumed to behave in a manner analogous to a cantilever beam with a nonuniform cross section, except that moments M_θ and forces N_θ are distributed along the sides. The mechanism of deformation and the yield condition are assumed unaffected by the longitudinal force (actually the radial component of force N_r) in the cantilever. For moderate deflections and for R/a ratios that are not large this assumption seems reasonable, especially in the outer regions of the plate. A yield condition is imposed consisting of an interaction between the circumferential components of bending moment M_θ and membrane force N_θ in the form

$$M_\theta/M_0 + (N_\theta/N_0)^2 = 1 \quad (19)$$

where $N_0 = \sigma_0 d$ is the fully plastic thrust. This represents an interaction of M_θ and N_θ acting on the cross section of an elemental ring of the plate in a manner similar to a beam subjected to bending and an axial thrust.[4] The flow rule associated with (19) is

$$\epsilon_\theta/\varkappa_\theta = 2M_0N_\theta/N_0^2 \quad (20)$$

where ϵ_θ is the circumferential component of strain.

The mechanism of the bending solution is kept, but a further assumption is made in order to simplify the analysis. In (20), ϵ_θ and $\varkappa_\theta$ depend on the shape of the deformed plate, so it is assumed that the shape of the annular part of the plate outside of the hinge circle can be approximated by a shallow cone; experimental results indicate that this assumption is not unreasonable. In this way, ϵ_θ and $\varkappa_\theta$ can be obtained readily as functions of the deformation angle φ and radius r. The deformation angle φ (Fig. 4) is taken to be the angle between the chord joining the point $r = \rho$ to $r = R$ at each meridional section. Using the shallow cone (φ small) approximation,

$$\epsilon_\theta = -(r - \rho)\varphi^2/2r \qquad \varkappa_\theta = \varphi/r \qquad \rho \leq r \leq R \quad (21)$$

Substituting the expressions (21) into the flow rule (20) gives the circumferential thrust $N = -N_\theta$ in the form

$$N = N_0(r - \rho)\varphi/d \qquad \rho \leq r \leq R \quad (22)$$

Eliminating N between (19) and (22) gives

$$M_\theta = M_0[1 - (r - \rho)^2\varphi^2/d^2] \qquad \rho \leq r \leq R \quad (23)$$

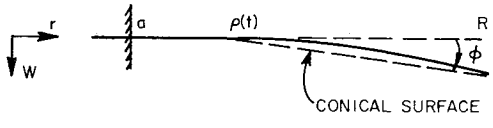

Fig. 4 Shallow cone approximation.

The remaining distribution of moments is taken as

$$0 \leq M_r \leq M_0 \qquad \rho \leq r \leq R$$
$$M_r = M_\theta = M_0 \qquad a \leq r \leq \rho \quad (24)$$

which is similar to that of the bending solution.

Using the results (22–24) and the shallow cone approximation, the angular momentum equation [corresponding to (8) of the bending solution] is

$$M_0[R + (R - \rho)^3\varphi^2/d^2] = m[\omega\rho F(\rho) - \dot{\omega}G(\rho)] \quad (25)$$

although the linear momentum equation remains as (7). Again $F(\rho)$ and $G(\rho)$ are given by expressions (9) and (10). Eliminating ω between (7) and (25) yields

$$R + (R - \rho)^3\varphi^3/d^2 = \frac{-I_2(R^2 - R_0^2)\dot{\rho}H}{4M_0(2R + \rho)^2} \quad (26)$$

in which $H = (R - \rho)^2 - 6R(R - \rho) + 6R^2$.

The deformation angle or cone angle φ is approximately the edge deflection divided by the length of the rotating generator $R - \rho$. Hence

$$\varphi = \frac{1}{R - \rho}\int_0^t (R - \rho)\omega dt = \frac{1}{R - \rho}\int_{R_0}^{\rho} (R - \rho)\omega\frac{d\rho}{\dot{\rho}} \quad (27)$$

Introducing the dimensionless variable $\eta = 1 - \rho/R$ converts the set of equations (7, 26, and 27) to be solved into

$$\omega = 3I_2(R^2 - R_0^2)/mR^3\eta^2(3 - \eta) \quad (28)$$

$$1 + R^2\varphi^2\eta^3/d = I_2(R^2 - R_0^2)h(\eta)\cdot\dot{\eta}/4M_0(3 - \eta)^2 \quad (29)$$

$$\varphi = \frac{1}{\eta}\int_{\eta_0}^{\eta} \eta\omega\frac{d\eta}{\dot{\eta}} \quad (30)$$

where $\eta_0 = 1 - R_0/R$ and

$$h(\eta) = \eta^2 - 6\eta + 6 \quad (31)$$

Substituting ω from (28) and $\dot{\eta}$ from (29) into the integrand of (30) gives

$$\varphi = \frac{\alpha}{\eta}\int_{\eta_0}^{\eta} \frac{h(\eta)d\eta}{\eta(3 - \eta)^3(1 + R^2\varphi^2\eta^3/d^2)} \quad (32)$$

where

$$\alpha = 3I_2^2(R^2 - R_0^2)^2/4mM_0R^3 \quad (33)$$

For $N < N_0$, (32) determines φ as a function of η and hence of ρ. From formula (22), $N < N_0$ for $(r - \rho)\varphi/d < 1$. In the initial motion φ increases, and, if the impulse is large enough, eventually $(R - \rho)\varphi/d = 1$. When this occurs, $N = N_0$ at the rim of the plate, and, during further deformation, the "conical" part of the plate has two annular regions separated by the circle of radius $r = \bar{r}$ determined by $(\bar{r} - \rho)\varphi/d = 1$. In the outer region where the fully plastic thrust has developed $N = N_0$, although in the inner region N is given by formula (22). The phase of motion or deformation, before the fully plastic thrust is developed, will be called phase 1a, and that, when it has developed, will be called phase 1b. Phase 1b ends when the plastic hinge circle reaches the support. Note that the condition $(R - \rho)\varphi < d$ that is necessary in phase 1a means that the edge deflection is less than the plate thickness.

An approximate solution of (32) now will be found. During phase 1a, $(R\varphi/d)\eta \leq 1$ so that $(R\varphi/d)^2\eta^3 \leq \eta \leq 1$. If the impulse is large enough, it is reasonable to expect $\eta = 1 - \rho/R$ to remain small. In other words, the hinge circle will not have traveled far before $N = N_0$. This assumption allows the approximation $[1 + (R\varphi/d)^2\eta^3]^{-1} \approx 1 - (R\varphi/d)^2\eta^3$. Small η also allows the approximation $h(\eta)(3 - \eta)^{-3} \approx \frac{2}{9}$. Hence Eq. (32) may be replaced by

$$\psi = \frac{2\alpha}{9}\int_{\eta_0}^{\eta} (1 - \beta\eta\psi^2)\frac{d\eta}{\eta} \quad (34)$$

where for brevity $\psi = \eta\varphi$ and $\beta = (R/d)^2$. Note that $R\psi$ is the edge deflection of the plate.

The first and second iterative solutions of (34) are

$$\left.\begin{aligned} \psi &= (2\alpha/9)\log(\eta/\eta_0) \\ \psi &= (2\alpha/9)\log(\eta/\eta_0) - (8\alpha^3\beta/729)[\eta\log^2(\eta/\eta_0) - \\ &\qquad 2\eta\log(\eta/\eta_0) + 2(\eta - \eta_0)] \end{aligned}\right\} \quad (35)$$

Phase 1a ends when $R\psi = d$. At this event let $\eta = \eta_1$. The value of η_1 is therefore determined from (35) after setting $\psi_1 = d/R = \beta^{-1/2}$. In particular, should the first iteration be adequate, $\eta_1 = \eta_0 e^{9d/2\alpha R}$.

Phase 1b describes the motion, although the region outside of the hinge circle is divided into two regions by the circle of radius $r = \bar{r}$ until $\rho = a$. For $\bar{r} \leq r \leq R$, $N = N_0$ and $M_\theta = 0$, and for $a \leq r \leq \bar{r}$ formulas (22) and (23) hold. This new distribution of forces and couples on a unit sector gives rise to the following angular momentum equation in terms of η [after eliminating ω from (7)] and replaces (29):

$$1 - \eta + 2R\varphi\eta^2/d = I_2(R^2 - R_0^2)h(\eta)\dot{\eta}/4M_0(3 - \eta)^2 \quad (36)$$

The deformation angle φ is now

$$\varphi = \frac{\eta_1}{\eta}\varphi_1 + \frac{1}{\eta}\int_{\eta_1}^{\eta} \eta\omega\frac{d\eta}{\dot{\eta}} \quad (37)$$

where $\varphi_1 = d/R\eta_1$.

Substituting ω from (28) and $\dot{\eta}$ from (36) in (37) gives

$$\psi = \psi_1 + \alpha\int_{\eta_1}^{\eta} \frac{h(\eta)d\eta}{\eta(3 - \eta)^2(1 - \eta + 2R\psi\eta/d)} \quad (38)$$

where

$$\psi_1 = \dot{\eta}_1\varphi_1 = d/R \quad (39)$$

In order to obtain a simple approximate solution of Eq. (38) it will be assumed that, during phase 1b, the plate deforms in such a way that the deformation angle φ varies little from the value φ_1. This approximation allows ψ to be found explicitly[5] in terms of η. However, for further simplification, it will again be assumed that $h(\eta)(3 - \eta)^{-3} \approx \frac{2}{9}$. The error is at its worst toward the end of phase 1b when, for the values $\frac{1}{4}$ and $\frac{5}{12}$ for the ratios a/R used in the experiments, the respective errors are about 18 and 9%. The error involved in finding ψ from (38) is much smaller because of the behavior of the weighting functions of $h(\eta)(3 - \eta)^{-3}$ in the integrand. A short discussion on the approximations used is contained in the Appendix. With the preceding two approximations, the solution of Eq. (38) is [set $\psi = \psi_1$ from (39) in integrand of (38)]

$$\psi = \psi_1 + (\alpha/9)[\log(\eta^2 f_1/\eta_1^2 f) + (4b - 1)^{-1/2}(\tan^{-1}c - \tan^{-1}c_1)] \quad (40)$$

where $b = 2R\varphi_1/d = 2\eta_1$, $f = 1 - \eta + b\eta^2$, $f_1 = 1 - \eta_1 + b\eta_1^2 = 1 + \eta_1$, $c = (2b\eta - 1)(4b - 1)^{-1/2}$, and $c_1 = 3(4b - 1)^{-1/2}$. Phase 1b ends when $\rho = a$, $\eta = \eta_2 = 1 - a/R$, $\varphi = \varphi_2$, and $\psi = \psi_2 = \eta_2\varphi_2$, the latter being obtained by setting $\eta = \eta_2$ in expression (40). The initial condition for phase 2, which is the angular velocity ω_2, is found by substituting $\eta = \eta_2$ in (28).

In phase 2, a sector is imagined to rotate about the support. The plate is still divided into two parts by the circle of radius $r = \bar{r}$ with a distribution of moments and forces similar to that in phase 1b. The new angular momentum equation is

$$1 - \eta_2 + 2R\varphi\eta_2^2/d = mR^3\eta_2^3(4 - \eta_2)\dot{\omega} \quad (41)$$

Noting that $\dot{\omega} = \frac{1}{2}d\omega^2/d\varphi$ and that $\omega(\varphi_2) = \omega_2$, given by (28) with $\eta = \eta_2$, the integration of (41) yields the relation

$$(\varphi_3^2 - \varphi_2^2)\eta_2^2 R/d + (\varphi_3 - \varphi_2)a/R = \theta \quad (42)$$

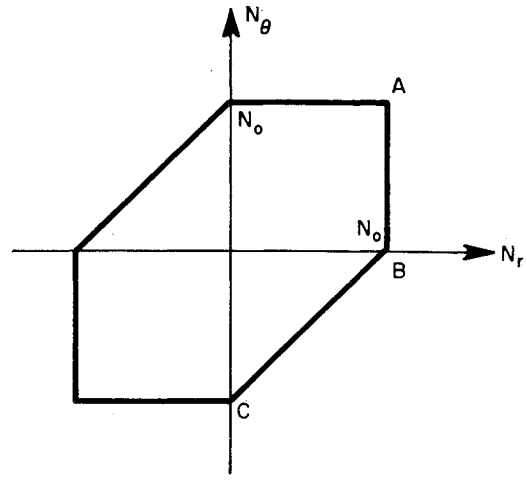

Fig. 5 Tresca yield hexagon.

where φ_3 is the deformation angle when motion ceases, that is, $\omega(\varphi_3) = 0$, and $\theta = \theta(r, t_f) - \theta(r, t_s)$, given by formula (15), is the rotation of unit sectors about the support during phase 2 in the bending solution. The final permanent edge deflection of the plate is

$$\delta = (R - a)\varphi_3 \quad (43)$$

where φ_3 is the solution of (42). In (42), φ_2, θ, and η_1 are given by (40, 15, and 35), respectively.

Membrane Solution

Bending stresses are now considered negligible compared with the membrane stresses. The mechanism of the bending solution is used along with the assumption that the shape of the plate outside of the hinge circle can be approximated by a shallow cone. The Tresca yield condition in terms of the membrane components N_r and N_θ is shown in Fig. 5.

At the edge of the plate $N_r = 0$, and, since the plate is forced into circumferential compression there, the governing plastic regime is the vertex C. The side BC describes the state in some annular region extending inwards from the plate edge. In this region,

$$N_r - N_\theta = N_0 \quad (44)$$

When the deflections are not too large the approximate equation of equilibrium in the radial direction is

$$(\partial/\partial r)(N_r r) - N_\theta = 0 \quad (45)$$

Solving Eqs. (44) and (45) for N_r and N_θ leads to

$$\begin{aligned} N_r &= N_0\log R/r & R/e \leq r \leq R \\ N_\theta &= -N_0(1 - \log R/r) & R/e \leq r \leq R \end{aligned} \quad (46)$$

Results (46) hold until $r < R/e$, where e is the base of the Naperian logarithms. At $r = R/e$, the plastic regime is vertex B in Fig. 5, where $N_r = N_0$ and $N_\theta = 0$. This approximate solution, therefore, only applies to plates with $a/R > 1/e \approx 0.367$. In one of the two series of experiments discussed later, $a/R = 1.5/6 = 0.25$, which means that, in order to satisfy the equation of equilibrium (45) in the annulus $1.5 < r < 2.2$, the yield condition (44) is violated. For the approximation $N_\theta = -N_0(r - a)/(R - a)$, used later to simplify the analysis, the value of N_r rises to $1.5\,N_0$ at the support.

Since the mechanism of deformation is the same as that of the two previous solutions, the conservation of linear momentum during phase 1 is still expressed by Eq. (28). The new angular momentum equation, using N_θ from (46) acting

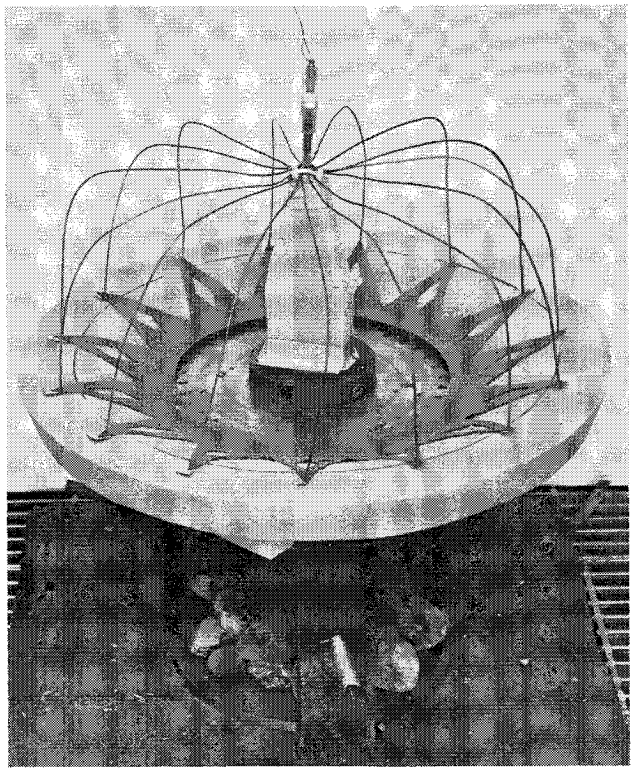

Fig. 6 Experimental arrangement.

on a unit sector of plate, is

$$-N_0\eta^2(3\eta_2 - \eta)\varphi/6\eta_2 = \frac{I_2(R^2 - R_0^2)h(\eta)\cdot\dot{\rho}}{4R^2(3 - \eta)^2} \quad (47)$$

where $h(\eta)$ is defined by (31). In the derivation of (47), ω was eliminated by using (28), and the approximation $1 - \log R/r \approx (r - a)/(R - a)$ was used to simplify the analysis.

The relation (27) may be expressed in the form $[\varphi(R - \rho)]^{\cdot} = (R - \rho)\omega$, in which the rate of the edge deflection is equated to the velocity at the edge. In terms of η this relation is

$$-\dot{\rho}(d/d\eta)(\eta\varphi) = \omega\eta R \quad (48)$$

Eliminating $\dot{\rho}$ between (47) and (48) leads ultimately to

$$\psi^2 = \frac{9I_2^2(R^2 - R_0^2)^2\eta_2}{mN_0R^4}\int_{\eta_0}^{\eta}\frac{h(\eta)d\eta}{(3\eta_2 - \eta)(3 - \eta)^3\eta^2} \quad (49)$$

Expanding the integrand in powers of η and noting that $\eta_0 \leq \eta \leq \eta_2 \leq 1 - 1/e \approx 0.63$, it is found that two terms give a reasonable approximation. Using only two terms then and carrying out the integration in (49) from η_0 to η_2 yields

$$\varphi_2^2 = \frac{2I_2^2(R^2 - R_0^2)^2}{3mN_0R^4}\cdot\frac{1}{\eta_2^2}\left[\frac{1}{\eta_0} - \frac{1}{\eta_2} + \frac{1}{3\eta_2}\log\frac{\eta_2}{\eta_0}\right] \quad (50)$$

Phase 2 with a stationary hinge circle at $r = a$ is governed by the angular momentum equation

$$(d/d\varphi)(\omega^2) = -[8N_0\varphi/m(3R + a)(R - a)] \quad (51)$$

where, in the derivation, the approximation $1 - \log R/r \approx (r - a)/(R - a)$ was again used. Setting $\eta = \eta_2 = 1 - a/R$ in (28) gives ω_2, the initial angular velocity for phase 2. Motion ceases when $\omega = 0$. Thus the final deformation angle φ_3, by the integration of (51), is determined by

$$\varphi_3^2 - \varphi_2^2 = \frac{9I_2^2(R^2 - R_0^2)^2(3R + a)}{4mN_0(R - a)^3(2R + a)^2}$$

and hence, using result (50) for φ_2^2,

$$\varphi_3^2 = \frac{I_2^2(R^2 - R_0^2)^2}{mM_0R^4\eta_2^2}\left[\frac{2}{3}\left(\frac{1}{\eta_0} - \frac{1}{\eta_2} + \frac{1}{3\eta_2}\log\frac{\eta_2}{\eta_0}\right) + \frac{9(4 - \eta_2)}{4\eta_2(3 - \eta_2)^2}\right] \quad (52)$$

The final edge deflection is therefore

$$\delta = (R - a)\varphi_3 \quad (53)$$

where φ_3 is determined by (52). Before comparing the deflections given by the three approximate theories, experiments are described against which all three can be compared.

Experiments

Description

Figures 6 and 7 show the experimental arrangement for applying transverse impulse loads around the rims of annular plates. Two series of experiments were conducted using 6061-T651 aluminum plates, 12 in. in diameter and $\frac{1}{4}$ in. thick. In one series the support radius was $1\frac{1}{2}$ in. in diameter, and in the other it was $2\frac{1}{2}$ in. The impulse was generated by sheet explosive† in the form of a $\frac{1}{2}$-in.-wide ring placed over a similar ring of solid neoprene attenuator, $\frac{1}{8}$ or $\frac{1}{4}$ in. thick to prevent spalling. To prevent the internal vertical spalls that occur under collisions of detonation fronts and to apply the loading as instantaneously as practicable, 16 triangular lead-in pieces of sheet explosive, 15 mils thick, located outside of the plate and supported on a styrofoam annulus (Fig. 7), were glued to the ring of explosive over the plate. These triangles of lead-in explosive were simultaneously detonated at the apices with 5-grain mild detonating fuse.

The edge deflections recorded were averages of the deflections taken at many points around the plate. This

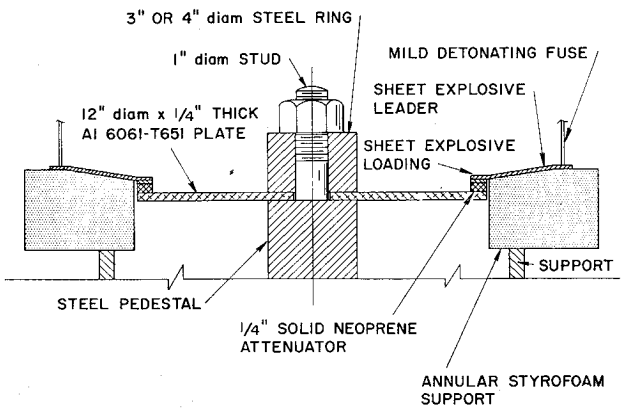

Fig. 7 Experimental arrangement.

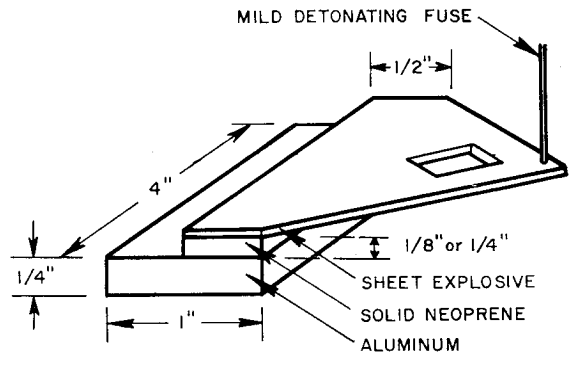

Fig. 8 Impulse calibration arrangement.

† DuPont sheet explosive EL-506D.

Table 1 Experimental and theoretical edge deflections

Support radius a, in.	Experiment no.	Impulse I_2, lb-sec/in.^{2}	δ_{ex}, in.	δ_1, in.	δ_2, in.	δ_3, in.	$\frac{\delta_{ex}}{\delta_1}$	$\frac{\delta_{ex}}{\delta_2}$	$\frac{\delta_{ex}}{\delta_3}$
1.5	1	0.200	0.20	0.492	...[a]	0.711	0.406	...[a]	0.281
	2	0.194	0.27	0.464	...	0.687	0.582	...	0.393
	3	0.207	0.26	0.532	...	0.735	0.489	...	0.354
	4	0.207	0.35	0.532	...	0.735	0.658	...	0.476
	5	0.292	0.50	1.050	0.563	1.036	0.476	0.880	0.482
	6	0.330	0.60	1.348	0.654	1.171	0.445	0.917	0.512
	7	0.402	0.79	2.011	0.846	1.427	0.393	0.934	0.554
	8	0.402	0.79	2.011	0.846	1.427	0.393	0.934	0.554
2.5	1	0.231	0.285	0.595	0.430	0.827	0.479	0.663	0.345
	2	0.316	0.530	1.113	0.616	1.131	0.476	0.860	0.469
	3	0.318	0.350	1.127	0.623	1.139	0.310	0.562	0.307
	4	0.363	0.470	1.474	0.741	1.300	0.319	0.634	0.362
	5	0.473	0.545	2.486	1.076	1.693	0.219	0.506	0.322

[a] These values are missing, because the impulse was not large enough to bring about phase lb. The experimental data are: the material, Aluminum 6061-T651; the yield stress σ_0, 44,700 psi; the plate density ρ, 0.000253 lb-sec^2/in.^{4}; the plate thickness d, $\frac{1}{4}$ in.; the plate outside of radius R, 6 in.; the plate support radii a, $1\frac{1}{2}$, and $2\frac{1}{2}$ in.; and the inner radius of loading R_0, $5\frac{1}{2}$ in.

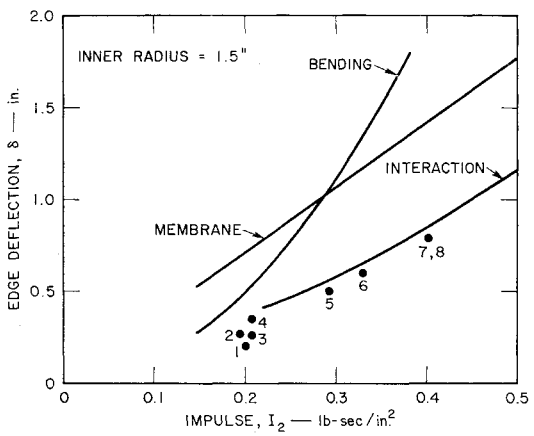

Fig. 9 Impulse vs edge deflection.

averaging was necessary, because the plates exhibited a small amount of buckling.

Standard American Society for Testing Materials (ASTM) tensile tests were run in an Instron machine with specimens taken along and across the rolling direction. The yield stress was chosen as the value at the point of intersection of the two straight lines approximating the elastic and strain-hardening portions of the stress-strain curve. It was found that the values of the yield stress along and across the rolling direction were within 2% of each other, and consequently the average value was taken. 6061-T651 aluminum was chosen because it exhibits little strain-hardening and is strain-rate insensitive.

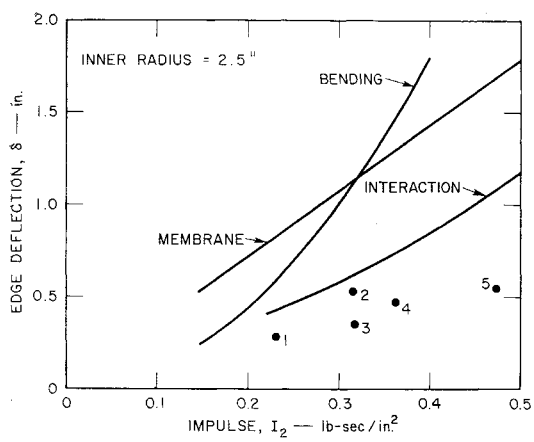

Fig. 10 Impulse vs edge deflection.

In order to determine the impulses corresponding to a given explosive-attenuator-target configuration, aluminum rectangular bars 4 in. long, 1 in. wide, and $\frac{1}{4}$ in. deep were projected in front of an x-ray camera, the configuration, shown in Fig. 8, being similar to that employed in the plate experiments. Two x-ray photographs taken at a known time interval apart determined the vertical component of velocity, and hence, knowing the mass of the plate, determined the impulse.

Results

The results of the two series of plate deflection experiments, differing only in the value of the support radius, are shown in Table 1 and Figs. 9 and 10.

In Table 1, δ_{ex} is the experimental edge deflection and δ_1, δ_2, and δ_3 are those predicted by the bending interaction, and membrane theories, respectively. They are given by formulas (18, 43, and 53).

Observations

From the results in Table 1 and Figs. 9 and 10, the following observations are made:

1) The bending theory greatly overestimates the edge deflections when they are about twice the plate thickness and tends to become more inaccurate for larger deflections, because membrane forces become more important. The theory seems satisfactory for deflections about the same as the plate thickness, although more experiments would be required to substantiate this observation.

2) The approximate limited-interaction theory is much better than the bending theory for predicting large edge deflections. It can be seen in Figs. 9 and 10 that the curves labeled "interaction" follow the trend of experimental points better than those curves labeled "bending." This is to be ex-

Table 2 Maximum values of M_r and N_r

a/R	I_2, lb-sec/in.^{2}	M_r/M_0	N_r/N_0 (at $r = a$)
0.417	0.221	1.000	0.975
	0.295	1.000	1.092
	0.368	1.089	1.148
	0.442	1.238	1.174
	0.516	1.389	1.181
0.250	0.221	1.000	2.118
	0.295	1.141	2.365
	0.368	1.403	2.484
	0.442	1.710	2.559
	0.516	1.994	2.592

Table 3 Numerical approximations

I_2, lb-sec/in.^{2}	η_1	$(1+\eta_1)^{-1}$	$1-\eta_1$	$\frac{h(\eta_1)}{(3-\eta_1)^3}$	$\frac{2}{9}$	$\eta_1^{(1)} = \eta_0 e$ $9d/2\alpha R$	$a = 1\frac{1}{2}$			$a = 2\frac{1}{2}$		
							δ_2	$\delta_2^{(1)}$	$\delta_2^{(2)}$	δ_2	$\delta_2^{(1)}$	$\delta_2^{(2)}$
0.221	0.328	0.753	0.672	0.217	0.222	0.362	0.416	0.413	0.430	0.411	0.408	0.419
0.295	0.188	0.842	0.812	0.221	0.222	0.192	0.575	0.567	0.612	0.574	0.566	0.599
0.368	0.142	0.876	0.858	0.221	0.222	0.142	0.768	0.754	0.786	0.770	0.756	0.786
0.442	0.121	0.892	0.879	0.222	0.222	0.120	0.995	0.973	0.993	0.997	0.976	0.980
0.516	0.110	0.901	0.890	0.222	0.222	0.109	1.256	1.225	1.194	1.257	1.228	1.174

pected as the interaction theory takes into account a membrane action. The excellent agreement that occurs in the first series (Fig. 9) is fortuitous. This is mainly caused by the omitted plate strength from elastic, strain-rate, and strain-hardening effects being compensated for by the restrictive yield condition imposed (no N_r, N_θ interaction) and probably by the effects of the shallow cone assumption. The second series (Fig. 10) is more realistic because the larger a/R ratio does not allow the radial component of the membrane force to build up so much, thereby diminishing its role. For this reason, although there are no experiments to prove it, it is believed that the interaction theory would come closer to reality for higher a/R ratios than those employed here.

3) The approximate membrane theory provides better deflection predictions than does the bending theory whenever the deflections are larger than four times the plate thickness. The curves labeled "membrane" in Figs. 9 and 10 follow the trend of experimental points with a continuing improvement of the values of the ratios δ_{ex}/δ_3 in the first series ($a = 1\frac{1}{2}$ in.) as the impulse increases. The predictions are not as good as those of the interaction theory, but the membrane theory does have the advantage of simplicity in the form of result (53). The interaction curve lies below the membrane curve, because the circumferential component of membrane force N_θ in the former is allowed to take on the value of the fully plastic thrust N_0 in the region $\bar{r} < r < R$ ($M_\theta = 0$ in this region) when the deflection is large enough. In the membrane solution, however, the interaction between N_θ and N_r keeps N_θ below N_0 except at the rim. Furthermore, for the a/R ratios used here, the interaction solution leads to values of N_r and M_r (from the equilibrium equations) that are in excess of the fully plastic thrust and moment. This situation is worst for low a/R ratios and high impulses. To give an idea of the range some maximum values are listed in Table 2.

4) The procedure adopted here of splitting up complicated problems, although not providing "exact" solutions, does provide results believed to be adequate for many engineering purposes.

Appendix

Numerical Approximations

To give some idea of the importance of the numerical approximations used in the limited interaction problem, Table 3 has been compiled. In obtaining the solutions (35) of Eq. (32), which describes phase 1a where $\eta_0 \leq \eta \leq \eta_1$, two numerical approximations were made. The first is $[1 + (R\varphi/d)^2\eta^3]^{-1} \approx 1 - (R\varphi/d)^2\eta^3$. It relies on η being small and is at its worst when $\eta = \eta_1$ when this approximation becomes $(1+\eta_1)^{-1} \approx 1 - \eta_1$. The second approximation is $h(\eta)(3-\eta)^{-3} \approx \frac{2}{9}$ and is also at its worst when $\eta = \eta_1$. Comparisons can be made using Table 3 for the plates and range of impulses considered here.

In obtaining the solution (40) of Eq. (38), two approximations were made. In the first, the value of φ in the integrand of (38) was taken constant at $\varphi = \varphi_1$, its initial value in phase 1b. The second approximation was again $h(\eta)(3-\eta)^{-3} \approx \frac{2}{9}$ and was made only to provide the simple solution (40). The edge deflections using these approximations are listed in Table 3 under δ_2. If the second approximation is not made, the edge deflections $\delta_2^{(1)}$ result.[5]

If the integral (38) is evaluated by using $\varphi = \varphi_1$ in the integrand, and the resulting function φ (from Simpson's quadrature) then approximated by means of two straight lines and again inserted in the integrand as a crude form of iteration, use of the new φ (again from Simpson's quadrature) leads to the edge deflections $\delta_2^{(2)}$. For the ranges of parameters used here, Table 3 shows no significant difference between the various deflections δ_2.

Finally in the interaction solution it is interesting to note that for most values of impulse the first iteration $\eta_1^{(1)}$ for the solution of (34) is adequate (Table 3). In these cases, η_1 is obtainable explicitly and is expressed by (35).

In the membrane solution the approximation $1 - \log R/r \approx (r-a)/(R-a)$ was used. The effect is to predict higher deflections than those of the theory without the approximations.

References

[1] Hopkins, H. G. and Prager, W., "On the dynamics of plastic circular plates," J. Appl. Math. Phys. **V**, 317–330 (1954).

[2] Wang, A. J. and Hopkins, H. G., "On the plastic deformation of built-in circular plates under impulsive load," J. Mech. Phys. Solids **3**, 22–37 (1954).

[3] Shapiro, G. S., "On a rigid-plastic annular plate under impulsive load," Prikl. Mat. Mekh. **23**, 172–175 (1959).

[4] Hodge, P. G., Jr., *Plastic Analysis of Structures* (McGraw-Hill Book Co., Inc., New York, 1959), Chap. 7, p. 170.

[5] Abrahamson, G. R., Lindberg, H. E., and Florence, A. L., "Investigation of response of simplified ICBM-type structures to impulsive loading," Air Force Special Weapons Center, New Mexico, AFWL-TRD 64-22, Contract AF 29(601)-4329, Stanford Research Institute (July 1964).